Producing Bessel Beams with an RF Transformer

Jian-yu Lu, *Life Fellow*, *IEEE*

***Abstract*— Bessel beams are exact solutions to the isotropic/homogeneous wave equation. In theory, they can propagate to infinite distance without diffraction. In practice, when produced with a finite aperture, they have a very large depth of field, i.e., they can maintain a small beamwidth over a large distance. In addition, they have a self-healing ability after encountering an obstacle. Because of these properties, Bessel beams have applications in optics, electromagnetics, ultrasound, quantum communications, electron beam guidance, and so on. Previously, in ultrasound, Bessel beams were produced with an annular array transducer driven by multiple independent high-voltage radio-frequency (RF) power amplifiers that were bulky, heavy, and consumed a lot of power, which limits the Bessel beams in applications such as wearable medical ultrasound imaging and wearable super-resolution imaging. In this paper, pulse (broadband) Bessel beams were produced by a single high-voltage RF power amplifier in combination with an RF transformer, reducing the size, weight, and power consumption. Experiments were performed to produce the pulse Bessel beams in water with a custom RF transformer and a custom 10-ring, 50-mm diameter, 2.5-MHz center frequency, and broadband (about 72% -6 dB relative one-way bandwidth) 1-3 lead zirconate titanate (PZT) ceramic/polymer composite annular array transducer driven by a commercial RF power amplifier at about +/-90 V. The results show that the pulse Bessel beams produced were very close to those generated with 10 independent high-voltage RF power amplifiers, computer simulations, and theory, and the pulse Bessel beams had a -6 dB beamwidth of about 2.53 mm (4.22 wavelengths) and a depth of field of about 216 mm (360 wavelengths). The reduced number of high-voltage RF power amplifiers makes it easier to apply Bessel beams in applications such as wearable medical ultrasound imaging and wearable super-resolution imaging, as is illustrated in examples where three-dimensional (3D) or multi-plane images can be produced using a Bessel beam and a mechanically scanned, multi-directional vibrating reflector.**

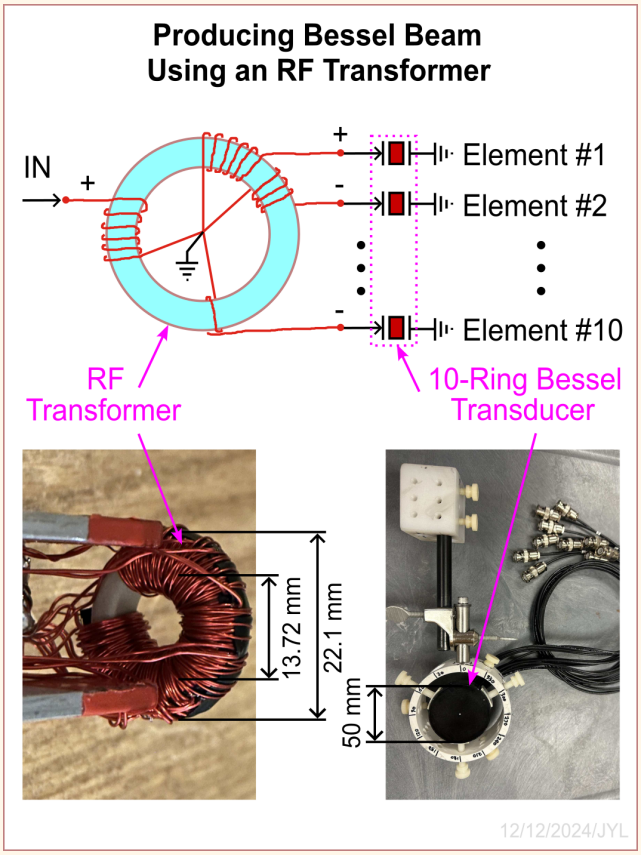

***Index Terms*— 2D and 3D imaging, Bessel beams, depth of field, electromagnetic, mechanical scanning, medical imaging, multi-directional reflector, multi-plane imaging, optics, radio frequency (RF), reflector, RF power amplifier, RF transformer, super-resolution imaging, ultrasound, ultrasound imaging, wearable imaging.**

I. Introduction

Bessel beams are exact solutions to the isotropic/homogeneous wave equation. They were first described by Julius A. Stratton in his book in 1941 [1]. In 1987, Durnin et al. studied the Bessel beams and performed an experiment in optics to produce these beams [2]-[4]. In theory, Bessel beams can propagate to infinite distance without lateral spreading of the beams (diffraction free). In practice, when realized with a finite aperture, these beams have a large depth of field (maintaining a small beamwidth over a large distance) [5]. In addition, these beams can heal themselves (self healing) after encountering an obstacle [6]. Because of these properties, Bessel beams have many applications in, for example, medical ultrasound imaging [5][7]-[8], optical imaging (such as optical coherence tomography or OCT) [9], photoacoustic imaging [10], blood flow velocity vector imaging [11], tissue property identifications [12], nondestructive evaluations (NDE) of materials [13], construction of new beams by orthogonal bases

Jian-yu Lu is with the Department of Bioengineering, The University of Toledo, Toledo, Ohio 43606, USA. (e-mail: jian-yu.lu@ieee.org).

Highlights

- **A single RF power amplifier in combination with a radio-frequency (RF) transformer was used to drive an annular array transducer to produce pulse Bessel beams that have a very large depth of field.**
- **Experiment results show that the method can produce pulse Bessel beams that are very close to those generated with multiple RF power amplifiers, computer simulations, and theory.**
- **The reduced number of high-voltage RF power amplifiers makes it easier to apply the Bessel beams to wearable medical ultrasound imaging, wearable super-resolution imaging, and other applications.**

[14], ultrasound therapy [15], acoustical [16] and optical [17] trapping of small particles over a large distance without losing focus, acoustic holograms [18], super-resolution optical imaging [19], optical light-sheet microscopy [20], optical material processing such as precision laser cutting [21], optical communications that resist turbulence [22], quantum communications [23], quantum entanglement [24][25], electron beam guidance [26], laser-driven accelerators [27], and electromagnetic waves [28].

Bessel beams can be produced by various methods. For example, in optics, Axicon Lens was used to produce Bessel beams approximately in a certain range away from the lens (the sidelobes of the produced beams are high near the surface of the lens and the intensity of the beam is not constant over the distance) [29]. Fourier method was used to produce Bessel beams [30]. In this method, a ring mask was placed at the focal distance of a lens and a Bessel beam was produced via a Fourier transform of the ring that was illuminated by a plane wave. However, this method has low energy efficiency since only a small amount of light can pass through the narrow ring slit. Spiral phase plate (SPP) was used to produce spiral or vortex Bessel beams [31] that are similar to the higher-order Bessel beams (see Eq. 10 in Ref. [32]). However, the intensity of such beams is zero on the beam axis [5]. Spatial light modulator (SLM) with certain phase profiles was used to produce Bessel beams [33]. However, such device requires a complicated system to operate and the accuracy of the produced Bessel beams is limited. Bessel beams also can be produced by nonlinear effects where the amplitude can alter the phase of the wave [34]. This method relies on nonlinear properties of propagating media and thus its applications are limited. In addition, Bessel beams can be produced by coupling a specific mode of waves into an optical fiber or a waveguide [35]. However, such a method only produces the Bessel beams in a confined space.

In acoustics or ultrasound, there are also many methods to produce Bessel beams [5][36]. For example, A 2.5-MHz, 50-mm diameter, 10-ring, and broadband ultrasound annular array transducer was used to produce a zeroth-order Bessel beam for medical imaging in 1990 [5]. Also, a 2.25-MHz piezoelectric ceramic transducer poled nonuniformly in radial direction was used to produce a zeroth-order Bessel beam [37]. The construction of such transducer was complicated and, unlike the annular array transducer, it could not be used to produce different transmit and receive beams to reduce sidelobes in applications such as medical imaging [5][38]. A randomly distributed and spatial-density weighted two-dimensional (2D) array transducer was proposed to produce a Bessel beam [39]. However, this method requires many transducer elements [5][38]. The optical Axicon above was adapted to ultrasound to produce quasi Bessel beams with similar issues as in optics [40][41]. Holographic phase plates were used to produce Bessel beams [18]. However, this method works only in a narrower bandwidth since the phase shifts required are frequency dependent. Metamaterials have been used to make a lens to produce an 8-KHz quasi Bessel beam in the air in a computer simulation [42]. This approach was similar to that of an Axcon except that a point source was used to illuminate the lens made of metamaterials to form an Axicon wavefront to produce a Bessel beam approximately. In addition, a 2D array transducer was studied to produce and steer Bessel beams for pulse-echo medical imaging [43]. However, a 2D array transducer is expensive and requires complicated wiring and associated electronics due to a large number of elements.

Although various methods can be used to produce Bessel beams, for medical ultrasound imaging, the approach that uses an annular array transducer is most attractive since it has several advantages [5]. First, as mentioned before, the amplitude and phase of the signal of each ring of the annular array transducer can be flexibly controlled to produce different beams. For example, the annular array transducer can be used to produce a Bessel beam in both transmit and receive to maintain a uniform beamwidth or lateral resolution in a pulse-echo imaging, or it can be used to produce a Bessel beam in transmit and then be apodized in aperture to produce a dynamically focused beam such as a dynamically focused Gaussian beam in receive to reduce the sidelobes of the transmit Bessel beam and increase image contrast [5][7][38]. Second, by setting the widths and positions of the rings of an annular array transducer to be corresponding to those of the lobes of a Bessel function, the number of rings can be minimized (see the 10-ring annular array transducer in Ref. [5]) and thus the array is relatively simple to construct and wire. As a comparison, a 128x128 2D array transducer has 16,384 elements, and even a one-dimensional (1D) array transducer typically has 128 to 256 elements. With an annular array transducer of a small number of elements, a simpler and more compact digital beamformer can be developed for dynamic focusing in receive [5][38]. For example, the commercial Texas Instruments analog front-end (AFE) chip AFE5812 integrates 8 independent channels of low-noise preamplifiers, programmable attenuators, 65-megasample-per-second (MS/s) / 14-bit analog-to-digital (A/D) converters, digital in-phase/quadrature (I/Q) demodulators, and continuous-wave (CW) Doppler I/Q mixers - all within a

compact 9 mm × 15 mm footprint and a height of only 1.26 mm. This chip can be controlled using a small field-programmable gate array (FPGA) combined with an embedded digital signal processing (DSP) module for digital beamforming, helping to enable battery-operated wearable imaging devices [44]–[48]. Note that, unlike a 1D array transducer, an annular array transducer can focus a beam symmetrically around its axial axis; thus, its beam quality can be comparable to that of a 2D array transducer, despite having far fewer transducer elements. Third, Bessel beams produced by an annular array transducer can be broadband (i.e., they can have a short pulse length), which is important for a high axial resolution in pulse-echo imaging. Also, the lateral beamwidth (related to the lateral image resolution) of the Bessel beams produced with an annular array transducer is independent of the pulse length over a large depth of field. Fourth, the energy efficiency of producing Bessel beams with an annular array transducer is higher than that with a single-ring transducer since the active surface area of the annular array transducer is larger. Higher energy efficiency increases signal-to-noise ratio (SNR) and the penetration depth of the beams in objects such as the biological soft tissues. Fifth, the annular array transducer can produce Bessel beams starting from the surface of the transducer until the depth of field of the beams. This allows objects that are very close to the surface of the transducer to be imaged clearly.

Despite the advantages of producing Bessel beams with an annular array transducer, previously, each ring of the transducer was independently driven by a high-voltage radio-frequency (RF) power amplifier, consuming a lot of power since multiple such amplifiers were needed to drive the transducer [5][38]. Because of high power and high voltage, to avoid overheating and voltage breakdown, these amplifiers were bulky (had a large physical size and heavy weight), which limits the Bessel beams in wearable applications (i.e., in devices that can be battery operated and worn on the human body for an extended period of time) such as wearable medical ultrasound imaging [44]-[48] and wearable super-resolution imaging [49]-[52]. To reduce the size, weight, and power consumption, it is desired to use a single high-voltage RF power amplifier to produce Bessel beams. However, single power amplifier can normally drive a single-element transducer that can only focus at a fixed depth with a small depth of field, especially when the *f*-number (the focal distance divided by the aperture diameter) of the transducer is small. Outside the depth of field, the image quality is degraded quickly.

To address the issues above, in this paper, a method that uses a single high-voltage RF power amplifier in combination with an RF transformer to produce Bessel beams was developed. In the method, the single RF power amplifier was used to drive the primary winding of the RF transformer that had multiple secondary windings connected to respective rings of the annular array transducer mentioned above. The number of turns of each secondary winding was proportional to the absolute value of the peak of the corresponding lobe of a Bessel function and the phase of the winding (or the direction of winding) was determined by the sign of the lobe (note that only two phases, 0^{o} and 180^{o}, are needed to produce a Bessel beam) [5]. Since the RF transformer can be small and only a single high-voltage RF power amplifier is needed in the method, the overall size, weight, and power consumption of the electronics can be significantly reduced. This makes it easier to apply Bessel beams to wearable imaging applications [44]–[52], as well as to other applications such as ultrasound therapy [15], the production of a cylindrical ring-shaped radiation force [49]–[52], CW Doppler, and acoustical tweezers for trapping particles [16], where continuous waves or waves with a high duty cycle may be needed. In addition, the RF transformer naturally helps its electrical impedance matching with the annular array transducer. Note that since both the absolute value of the peak of the lobes of a Bessel function and the number of turns of each secondary winding of the RF transformer are proportional to $1/\sqrt{r}$ asymptotically, where r is the radial distance, the electrical impedances of both the secondary windings and the corresponding rings of the annular array transducer will be proportional to $1/r$ for outer rings. This is because the electrical impedance of a ring of an annular array transducer is inversely proportional to the area of the ring (assuming that a ring of the annular array transducer is bounded by radii r_1 and $r_2 > r_1$, its area will be $\pi(r_2^2 - r_1^2) = \pi(r_2 + r_1)(r_2 - r_1) \approx 2\pi r(\Delta r)$ or is proportional to r since Δr is almost a constant and $r_1 \approx r_2 \approx r$ if r is not too small).

To form an image, the Bessel beam produced by an annular array transducer needs to be scanned linearly or in a sector format using methods such as a linear stage, a wobbler [38][53], or a vibrating reflector [54][55]. Among these scanning methods, the vibrating reflector is particularly attractive for wearable applications because it can be lightweight and vibrate at a high frequency (e.g., 250 Hz or 500 frames per second (fps), with a potential to reach 2,000 Hz in the future; see Refs. [54][55]). Combined with the vibrating reflector, the Bessel beam can be used to produce real-time images of a large depth of field and strong self-healing ability (i.e., reducing shadows caused by objects such as hard tumors) [6][56]. Although the vibrating reflector has many advantages, its current design only allows it to vibrate in one direction, limiting imaging with the Bessel beam produced by an annular array transducer to 2D [54][55]. To enable three-dimensional (3D) or multi-plane imaging, methods that allow multi-directional vibration of the reflector were developed, and examples of wearable ultrasound imaging and super-resolution imaging systems using a Bessel beam and a multi-directional vibrating reflector are given.

The paper is organized as follows. The theory of Bessel beams is given in Section II. The experiment methods are in Section III. The results are in Section IV. Discussion and conclusion are given in Section V and VI respectively.

II. Theoretical Preliminary

A. Bessel Beam

The free space (or isotropic/bomogeneous) scalar wave equation in cylindrical coordinates is given by [32]:

$$\left[\frac{1}{r}\frac{\partial}{\partial r}\left(r\frac{\partial}{\partial r}\right)+\frac{1}{r^2}\frac{\partial^2}{\partial \phi^2}+\frac{\partial^2}{\partial z^2}-\frac{1}{c^2}\frac{\partial^2}{\partial t^2}\right]\Phi(r,\phi,z;t)=0\,, \quad (1)$$

where $r=\sqrt{x^2+y^2}$ represents the radial coordinate, ϕ is an azimuthal angle, z is an axial axis that is perpendicular to the plane defined by r and ϕ, $\vec{r}=(r\cos(\phi),r\sin(\phi),z)$ represents a spatial position, t is the time, c is the speed of sound or light, and $\Phi(r,\phi,z;t)$ (wave field) represents acoustic pressure or Hertz potential that is a function of r, ϕ, z, and t.

From Eq. (1), a family of solutions to the wave equation can be obtained (see Eq. (2) in Ref. [32]):

$$\Phi_{\varsigma}(s)=\int_0^{\infty}T(k)\left[\frac{1}{2\pi}\int_{-\pi}^{\pi}A(\theta)g(s)d\theta\right]dk\,, \quad (2)$$

where

$$s=\alpha_0(k,\varsigma)r\cos(\phi-\theta)+b(k,\varsigma)\left[z\pm c_1(k,\varsigma)t\right], \quad (3)$$

and where

$$c_1(k,\varsigma)=c\sqrt{1+\left[\alpha_0(k,\varsigma)/b(k,\varsigma)\right]^2}\,, \quad (4)$$

where k, ς, and θ are parameters that are independent of the spatial positions, ς is an Axicon angle [40][57], $T(k)$ is any complex function (well behaved) of k and could include the temporal frequency transfer function of a wave source, $A(\theta)$ is any complex function (well behaved) of θ and represents a weighting function of the integration with respect to θ, $g(s)$ is any complex function (well behaved) of s, and both $\alpha_0(k,\varsigma)$ and $b(k,\varsigma)$ are any complex functions of k and ς. Note that "$\pm$" in Eq. (3) represent backward and forward propagating waves, respectively. (In the following, we consider only the forward propagating waves.)

If $T(k)=\delta(k-k_0)$, where $\delta(k-k_0)$ is a Dirac-Delta function [58], $k_0=\omega_0/c>0$ is a constant that represents a wave number, $\omega_0=2\pi f_0$ is an angular frequency, f_0 is the frequency of the wave, $g(s)=e^s$, $\alpha_0(k,\varsigma)=-i\alpha$, $b(k,\varsigma)=i\beta=i\omega_0/c_1$ (see Eq. (3)), $i=\sqrt{-1}$, from Eqs. (2) and (3), one obtains Durnin's beam [2] (see Eq. (8) in Ref. [32]):

$$\Phi_D(s)=\left[\frac{1}{2\pi}\int_{-\pi}^{\pi}A(\theta)e^{-i\alpha r\cos(\phi-\theta)}d\theta\right]e^{i(\beta z-\omega_0 t)}\,, \quad (5)$$

where (see Eqs. (3) and (4))

$$\beta=\sqrt{k_0^2-\alpha^2}\,, \quad (6)$$

and where α is a constant and is a scaling parameter of the beam.

Note that since the integration in the square bracket in Eq. (5) is independent of the propagation distance, z, and the time, t, in theory, Durnin's beam does not spread or diffract in the transverse plane (r,ϕ) as the wave propagates to an infinite distance. However, since $c_1(k_0,\varsigma)=\omega_0/\beta$, the speed of wave of Durnin's beam in Eq. (5) depends on the wave number, k_0. Therefore, if $T(k)$ in Eq. (2) is a complex function containing multiple frequencies, $\Phi_{\varsigma}(s)$ will represent a dispersive wave (wave speed changes with the frequency) and its shape will change in the axial direction, z, as the wave propagates. To get waves that do not diffract in both transverse and axial directions as they propagate to an infinite distance, $c_1(k_0,\varsigma)$ in Eq. (2) must be a constant. X waves [32] or quantum X waves [59][60] are such waves that have a constant speed $c_1\geq c$, i.e., both the phase and group velocities of these waves are the same and are always larger than or equal to the speed of light in vacuum or the speed of sound in isotropic/homogeneous media.

If $A(\theta)=i^n e^{in\theta}$, we obtain the nth-order Bessel beams (see Eq. (10) in Ref. [32]):

$$\Phi_{J_n}(s)=J_n(\alpha r)e^{i(\beta z-\omega_0 t+n\phi)},\ n=0,1,2,\cdots, \quad (7)$$

where $J_n(\cdot)$ is the nth-order Bessel function of the first kind. Because the nth-order Bessel beam in Eq. (7) is zero on the beam axis unless $n=0$, in the remainder of this paper, we will only study the zeroth-order Bessel beam J_0 that is axially symmetric (i.e., not a function ϕ) and can be applied to medical imaging [5]:

$$\Phi_{J_0}(r,z)=J_0(\alpha r)e^{i(\beta z-\omega_0 t)}\,. \quad (8)$$

If α = 0, Eq. (8) represents a plane wave [2].

B. Depth of Field of Bessel Beam

Although Bessel beams can theoretically maintain their narrow transverse beam profiles over infinite distances, in practice, when produced with a finite aperture, they exhibit a very large depth of field [2]-[5]. The depth of field of a Bessel beam produced with a finite aperture is given by [2][8][59]:

$$DOF_B=\frac{D}{2}\sqrt{\left(\frac{k_0}{\alpha}\right)^2-1}\,, \quad (9)$$

where D is the diameter of the transducer. If the scaling parameter α = 1202.45 m^{-1}, center frequency f_0 = 2.5 MHz, speed of sound in water c = 1500 m/s, and D = 50 mm, the calculated DOF_B = 216.28 mm (about 360.47 λ, where $\lambda=c/f_0$ = 0.6 mm is the center wavelength). The full-width-at-half-maximum (FWHM) beamwidth of the Bessel beam is determined by the -6 dB width of the center lobe of the $J_0(\alpha r)$ Bessel function, which is about 2.53 mm (or 4.22 λ) with the α value above [5]. As a comparison, if the same annular array transducer is apodized to produce a Gaussian beam that has a 25-mm FWHM aperture at the surface of the transducer and is focused at z = 120 mm, its depth of field will only be about 24.4 mm (41 λ) [5]. As the FWHM aperture of the focused Gaussian beam is increased or the focal length is decreased (i.e., the *f*-number becomes smaller), the depth of field will be further reduced.

The large depth of field of the Bessel beams is beneficial to

medical imaging [5][7][38]. If a single-element transducer focused at a fixed distance is used in imaging, it will have a short depth of field in both transmit and receive as mentioned above and the lateral image resolution will decrease quickly away from the depth of field, especially when the *f*-number is small, leading to a poor image quality. Although the focal distance of an annular array transducer can be changed, it is still fixed in each transmission. Thus, to form an image of an effectively large depth of field, a montage of images obtained from multiple transmissions focused at different distances is needed. The montage process is to cut a strip of the image around each focal distance and then piece it together with the strips obtained from other focal distances, which takes time and thus reduces image frame rate. Also, unlike Bessel beams that can be produced with a single RF power amplifier in combination with an RF transformer, to focus a beam electronically in transmit with an annular array transducer, the electrical signals that drive the transducer need to be delayed precisely and thus multiple RF power amplifiers and complicated digital control circuits are needed.

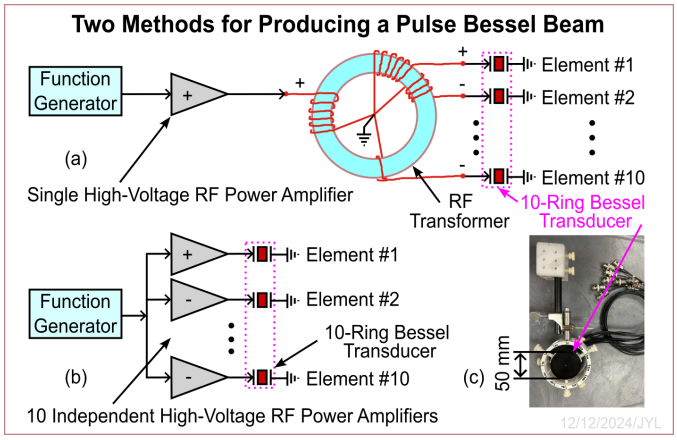

Fig. 1. Two methods to drive a 10-ring annular array transducer (Bessel transducer) to produce pulse Bessel beams. (a) Producing the Bessel beams with a single high-voltage radio-frequency (RF) power amplifier in combination with an RF transformer. (b) Producing the Bessel beams with 10 independent high-voltage RF power amplifiers. (c) A photo of the 10-ring annular array transducer. The "+" and "-" signs indicate 0° and 180° phase shifts respectively.

III. Experiment Methods

A. Bessel Transducer

To produce a Bessel beam experimentally in water, a custom 10-ring, 2.5-MHz center frequency, 50-mm diameter, and broadband (about 72% -6 dB relative one-way bandwidth) annular array transducer (Bessel transducer) was used [5]. The transducer was made of 1-3 lead zirconate titanate (PZT) ceramic/polymer composite material sandwiched between front matching and back absorbing layers. The width of each ring of the transducer was proportional to that of the corresponding lobe of the $J_0(\alpha r)$ Bessel function, where α = 1202.45 m^{-1}. The gap between adjacent rings was about 0.2 mm. The radii of the centers of the gaps were determined by the positions of the corresponding zeros of the $J_0(\alpha r)$ Bessel function. The depth of field and the FWHM beamwidth of the Bessel beam produced were about 216 mm (Eq. (9)) and 2.53 mm, respectivevly. A photo of the annular array transducer is shown in Fig. 1(c).

B. Production of Bessel Beams

A single RF power amplifier in combination with an RF transformer was used to produce Bessel beams (see Fig. 1(a), Fig. 2(a), and Fig. 2(b)). The RF transformer consisted of one primary winding of 45 turns of a Gauge 22 (0.644 mm diameter) magnetic wire and 10 secondary windings of integer approximations of 45.0, 18.1, 13.5, 11.2, 9.83, 8.84, 8.10, 7.52, 7.05, and 6.66 turns that were calculated by multiplying 45 with the absolute values of the peaks of the $J_0(\alpha r)$ Bessel function, i.e., 1.00, -0.4028, 0.3001, -0.2497, 0.2184, -0.1965, 0.1801, -0.1672, 0.1567, and -0.1480, respectively, for Rings #1 to #10 of the annular array transducer. If the peak value of the Bessel function was negative, the direction of the corresponding winding was reversed, producing a 180° phase shift. The magnetic wires used in the secondary windings had Gauge 28 (0.321 mm diameter) for Ring #1 and Gauge 24 (0.511 mm diameter) for Rings #2 to #9 for simplicity. The maximum output voltage of the power amplifier was set to about 90 Vp (peak voltage) and the amplifier was driven by a one-cycle 2.5-MHz electrical sine signal. Since the enamel on the magnetic wires can withstand at least 20 V/μm and the thickness of the enamel is usually more than 30 μm, these magnetic wires are safe to be used for a peak voltage of about 90 Vp (or 180 Vpp peak to peak) without additional insulations. The core of the transformer used had a toroidal shape and was made of Cobalt-Nickle-Zinc (CoNiZn) (11-780-K, Ferronics, Bethlehem, PA, USA). The outer (O.D.) and inner (I.D.) diameters of the toroidal core were 22.10 mm and 13.72 mm, respectively, and the height of the core was h = 6.35 mm. The self-inductance of a winding of a toroid can be calculated with (see Eq. 7.28 in Ref. [61] at P.325):

$$L = \frac{\mu_0 \mu_r M^2 h}{2\pi} \ln\left(\frac{\text{O.D.}}{\text{I.D.}}\right), \qquad (10)$$

where $\mu_0 = 4\pi \times 10^{-7}$ H/m is the permeability constant in vacuum, μ_r = 125 is the relative permeability of the toroidal core, and M is the number of turns. With M = 45 for the primary winding, the calculated self inductance was about 153.3 μH or an impedance of 2407.3 ohms at 2.5 MHz. This means that the transformer itself does not add a significant load to the RF power amplifier when there is no load to the secondary windings. If M is too large, there is a possibility to saturate the transformer with a large total magnetic field strength. Thus, M = 45 was selected as a compromise. Note that the size of the ferrite core above can be reduced if the average power is lower (i.e., when the duty cycle of the transmit pulses is low and/or the transducer has a smaller diameter), and the diameter of the magnetic wires can be decreased if the actual maximum current is smaller.

For comparison, the annular array transducer above was also driven by 10 independent high-voltage RF power amplifiers to produce Bessel beams (see Figs. 1(b), 2(c), and 2(d)). The output voltage of each RF power amplifier was

proportional to the absolute value of the peak of the corresponding lobe of the $J_0(\alpha r)$ Bessel function and the phase (0^o or 180^o) of the RF power amplifier was determined by the sign of the lobe (Fig. 1(b)).

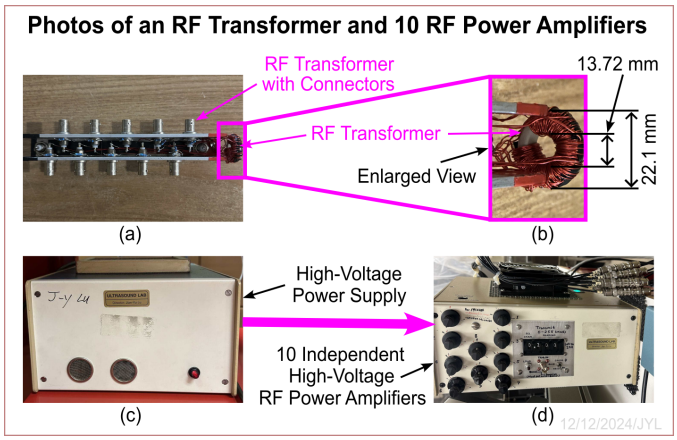

Fig. 2. Photos of the high-voltage RF power amplifiers and the RF transformer to drive the 10-ring annular array transducer to produce pulse Bessel beams. (a) The RF transformer and its Bayonet Neill-Concelman (BNC) connectors for the 10-ring annular array transducer. (b) Enlarged view of the RF transformer. (c) High-voltage DC power supply (about 229 mm (width) x 133 mm (height) x 229 mm (depth) in demensions). (d) 10 independent high-voltage RF power amplifiers (about 305 mm (width) x 137 mm (height) x 241 mm (depth) in dimensions) to drive the 10-ring annular array transducer.

C. Experiment System

Fig. 3 shows an experiment system for measuring pulse Bessel beams produced by the 10-ring annular transducer in Fig. 1(c). In the experiments, the annular array transducer and a broadband (1-20 MHz) polyvinylidene fluoride (PVDF) needle hydrophone (TNU001A, NTT Systems, Inc., Seattle, Washington, USA) of 0.6-mm diameter were placed in a water tank as shown on the right and left hand sides of Fig. 3(a) respectively. A block diagram of the experiment system is given in Fig. 3(b). During the experiments, a step motor moved (scanned) the annular array transducer along the x axis over a distance of 50 mm in 200 equal-distance steps (the step size was 0.25 mm) (since the motion between the hydrophone and the annular array transducer is relative, the hydrophone can be scanned instead). Since the Bessel beams were axially symmetric, only one scan across the axial axis of the annular array transducer was necessary to obtain entire pulse Bessel beams at an axial distance, z. At each scanning step, an unsynchronized trigger signal was generated by the motor unit and then sent to a digitizing unit to produce another trigger signal synchronized to the clock of the digitizer. The synchronized trigger was sent to a function generator (HP8116A, Hewlett-Packard Company, CA, USA) to produce a 1-cycle and 2.5-MHz electrical sine-wave signal that was sent to either 10 home-made independent high-voltage RF power amplifiers (Figs. 1(b), 2(c), and 2(d)) to drive the 10-ring annular array transducer or to a commercial RF power amplifier (ENI2100L, Electronics and Innovation, Ltd., NY, USA) to drive the RF transformer (Figs. 1(a), 2(a), and 2(b)) that was connected to the transducer. The ultrasound pulse Bessel beams produced in water were received by the PVDF needle hydrophone and the received signals were amplified, filtered by a 0.5-7.5 MHz band-pass filter, digitized at 50 MS/s and 12-bit resolution, and then stored on a hard disk.

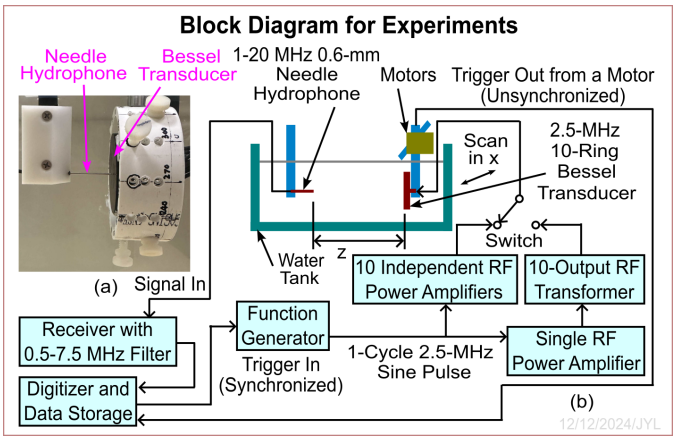

Fig. 3. Block diagram of the experiments. (a) A photo of the needle hydrophone and the 10-ring annular array transducer (Bessel transducer). (b) Block diagram of the experiments. The 10-ring annular array transducer was placed on the right hand side of the water tank. Pulse Bessel beams produced by the transducer was received by a broadband PVDF needle hydrophone (0.6-mm in diameter and 1-20 MHz bandwidth, see the left hand side of the water tank). To map the Bessel beams, the transducer was moved (scanned) along the x axis in multiple equal-distance steps and the tip of the needle hydrophone acrossed the axis of the transducer. At each step, an unsynchronized trigger signal was produced from the motor unit and sent to the digitizer unit that produced another trigger signal synchronized to the clock of the digitizer. The synchronized trigger was used to trigger a function generator to produce a 1-cycle and 2.5-MHz electrical sine signal that was amplified to drive the transducer to produce pulse Bessel beams. The Bessel beams were measured by the hydrophone to produce electrical signals that were amplified, filtered, digitized, and then stored in a hard disk. The switch indicates that the transducer can be driven either by a single high-voltage RF power amplifier in combination with an RF transformer or by 10 independent high-voltage RF power amplifiers.

IV. Results

Fig. 4 shows an analytic envelope of the RF pulse Bessel beams measured by the 0.6-mm broadband PVDF needle hydrophone at 3 axis distances, z = 1 mm (Figs. 4(a) and 4(d)), 100 mm (Figs. 4(b) and 4(e)), and 200 mm (Figs. 4(c) and 4(f)) from the surface of the annular array transducer using the experiment system in Fig. 3. Figs. 4(a) to 4(c) were obtained using the single high-voltage RF power amplifier in combination with the RF transformer above to drive the 10-ring annular array transducer. Figs. 4(d) to 4(f) are the same as Figs. 4(a) to 4(c) respectively, except that they were obtained with the 10 independent high-voltage RF power amplifiers (see Fig. 1(b), Fig. 2(c), and Fig. 2(d)). In each panel of Fig. 4, the vertical and horizontal dimensions represent the scanning distance (50 mm) of the annular array transducer in the water tank and the time (10.24 μs) respectively. The color bar on the right hand side of Fig. 4 represents a normalized magnitude of the measured acoustic pressure in water. As mentioned before, the scaling parameter, the center frequency, and the speed of sound for the pulse Bessel beams were α = 1202.45 m^{-1}, f_0

= 2.5 MHz, and c = 1500 m/s (or the center wavelength λ = 0.6 mm), respectively. It is clear from Fig. 4 that the pulse Bessel beams have a narrow FWHM mainlobe beamwidth (close to the theoretical value of 2.53 mm or 4.22 λ) and stay in focus from the surface of the transducer to over z = 200 mm (the depth of field calculated from Eq. (9) was about 216.28 mm or 360.47 λ). Figs. 4(a), 4(b), and 4(c) are similar to Figs. 4(d), 4(e), and 4(f), respectively.

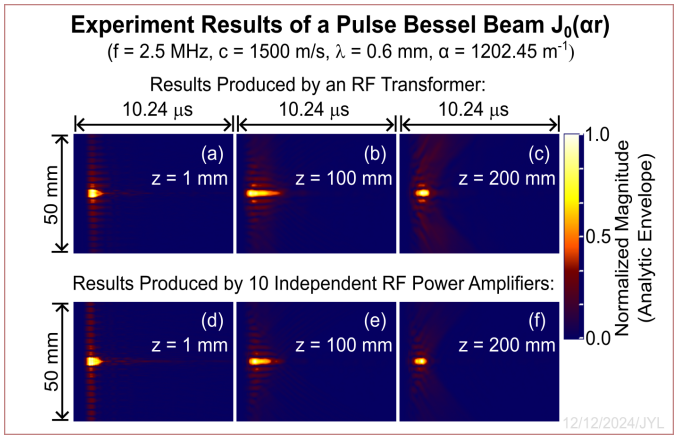

Fig. 4. Measured pulse Bessel beams at different axial distances using a single high-voltage RF power amplifier in combination with an RF transformer (top row) and using 10 independent high-voltage RF power amplifiers (bottom row) to drive a 10-ring annular array transducer. (a) and (d) Pulse Bessel beams measured at axial distance z = 1 mm from the surface of the transducer. (b) and (e) are the same as (a) and (d) respectively except that they were obtained at z = 100 mm. (c) and (f) are also the same as (a) and (d) respectively except that they were obtained at z = 200 mm. The pulse Bessel beams were produced by driving an annular array transducer with a 1-cycle electrical sine signal and were measured by scanning the annular array transducer along the x axis for 50 mm. The signals were received by a 0.6-mm broadband PVDF needle hydrophone and were digitized at 50 MS/s sampling rate and 12-bit resolution for 10.24 μs. The analytic envelope of the pulse Bessel beams was displayed and the color bar on the right indicates normalized magnitude.

Fig. 5 is the same as Fig. 4 except that an RF signal at each row is displayed. It can be seen that the results obtained with and without using an RF transformer are similar.

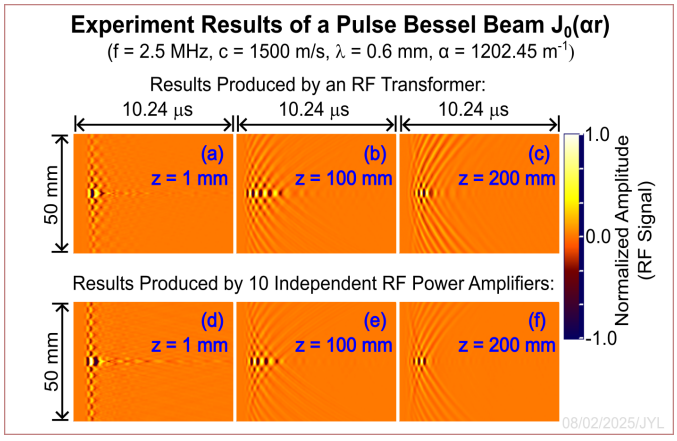

Fig. 5. This figure is the same as Fig. 4 except that an RF signal at each row is displayed. The color bar indicates normalized amplitude from -1.0 to 1.0. If the positive peak value is larger than the absolute value of the negative peak, the panel is normalized with the positive value. Otherwise, it is normalized with the absolute value of the negative peak.

Fig. 6 shows lateral (perpendicular to the axial axis) line plots of the pulse Bessel beams in Fig. 4 at three axial distances z = 1 mm (Fig. 6(a)), 100 mm (Fig. 6(b)), and 200 mm (Fig. 6(c)) from the surface of the annular array transducer. The solid (black) and dotted (red) lines correspond to the top (using a single high-voltage RF power amplifier in combination with an RF transformer) and bottom (using 10 independent high-voltage RF power amplifiers) rows of Fig. 4 respectively. The line plots were normalized to their respective maxima in vertical axis, and each line represents the maximum values (maximum sidelobes of the Bessel beams) of the rows in each panel in Fig. 4. For comparison, the following plots are also shown in the Fig. 6: simulated Bessel beam using parameters corresponding to those of the experiment except that exact Bessel aperture weighting was used (dashed lines in blue color); simulated pulse Gaussian beam (2.5-MHz center frequency) focused at z = 100 mm with a FWHM of 25 mm at the transducer aperture of 50-mm diameter (solid lines in pink color) (the bandwidth and the drive signal of the transducer were the same as those used to produce the simulated Bessel beam); and a plot of the $|J_0(\alpha r)|$ Bessel function (dash-dotted lines in cyan color), where α = 1202.45 m^{-1}. The simulations were performed with the method developed in Ref. [62] and implemented in C language on a Linux operating system. From the plots in Fig. 6, it is clear that the pulse Bessel beams produced with and without using multiple RF power amplifiers were very close, and they are also close to those produced by computer simulations or the theoretical Bessel function. As expected, a focused Gaussian beam has a small beamwidth only around its focal distance due to a short depth of field.

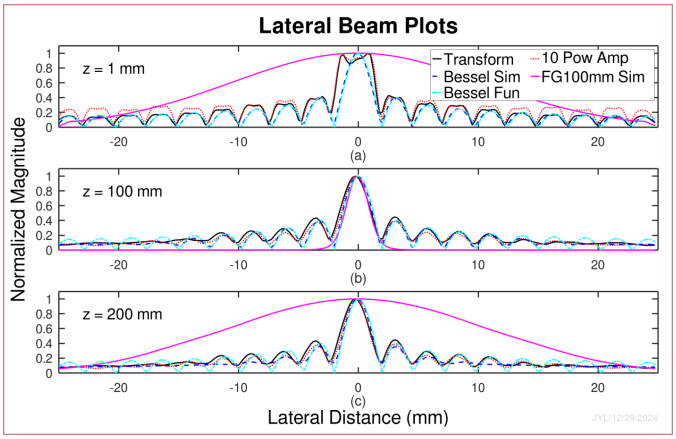

Fig. 6. Line plots of the pulse Bessel beams measured across the axial axis of the annular array transducer along the x axis (lateral distance) at (a) z = 1 mm, (b) z = 100 mm, and (c) z = 200 mm. The solid (black) and dotted (red) lines correspond to the top (using a single high-voltage RF power amplifier in combination with an RF transformer) and bottom (using 10 independent high-voltage RF power amplifiers) rows of Fig. 4 respectively. The line plots were normalized to their respective maxima in vertical axis, and each line represents the maximum values (maximum sidelobes of the Bessel beams) of the rows of each panel in Fig. 4. For comparison, the following plots are also shown in the figure: simulated Bessel beam

with parameters corresponding to those of the experiment except that exact Bessel aperture weighting was used (dashed lines in blue color); simulated pulse Gaussian beam focused at z = 100 mm with a FWHM of 25 mm at the transducer surface (solid lines in pink color); and a plot of the $|J_0(\alpha r)|$ Bessel function (dash-dotted lines in cyan color).

V. Discussion

It is seen from Figs. 4 and 5 that the pulse length of the Bessel beams changes with the axial distance z (a longer pulse length means a lower axial resolution in pulse-echo imaging. The elongation of the pulse length during the wave propagation was caused by the dispersion of the Bessel beams (i.e., the speed of the wave, $c_1 = \omega_0 / \beta$, changes with the frequency in the propagation term $e^{i(\beta z - \omega_0 t)} = e^{i\beta(z - c_1 t)}$ of Eq. (7) or Eq. (8)), especially when α approaches to k_0 and the depth of field is close to zero. To reduce dispersion, either a smaller α, which reduces lateral image resolution, or X waves that have a constant speed $c_1 = c/\cos(\varsigma) \geq c$ [32][59]-[60], can be used, where ς is the Axicon angle [40][57] and c_1 is both the phase and group velocities of the waves (since $c_1 \geq c$, X waves are superluminal in optics and supersonic in ultrasound). Note that to produce ultrasound X waves using an annular array transducer, multiple RF power amplifiers should be used since each transducer element needs to be driven by a different pulse waveform (see Section III on Page 23 in Ref. [32] for producing X waves with a finite aperture radiator) [38][63].

The piecewise amplitude weighting of the annular transducer can be clearly seen in Fig. 6(a) (see the black solid line and red dotted line). In addition, the Bessel beam produced by the 10 RF power amplifiers has higher sidelobes due to inaccurate settings of the voltages of the amplifiers (Fig. 6(a)). However, none of these variations near the surface of the transducer (z = 1 mm) affect much the Bessel beam measured in Fig. 6(b) (z = 100 mm) and Fig. 6(c) (z = 200 mm). Such variations of the amplitudes can be viewed as if the transducer were partially obstructed or altered near the center rings that boosted the relative sidelobes in outer rings. However, after some distance of propagation, the Bessel beams recover themselves. This is evident by comparing the measured Bessel beams with the simulated Bessel beam in blue dashed line and the theoretical Bessel function in cyan dash-dotted line in Fig. 6(a). Since a Bessel beam has almost the same lateral beam profile at any axial distance within its depth of field, the Bessel beams are expected to recover themselves after some distance of propagation even the partial obstruction appears at other axial distances. This is similar to what it is called "self-healing" properties of a class of beams such as Bessel beams, X waves, and Airy beams that have relatively high sidelobes [6][56]. I.e., when one part of the beam is obstructed, the remaining energy in the sidelobes can reconstruct the beam after the obstacle. Self healing will reduce the shadows cast behind objects such as hard tumors in medical ultrasound imaging [56].

The pulse lengths of the pulse Bessel beams in the top and bottom rows of Figs. 4 and 5 have some difference at each axial distance, z. For simplicity, there was no dedicated electrical impedance matching network used for each ring of the annular array transducer in the experiments. Using a wideband electrical impedance matching network to reduce the reflection of the electrical energy between the transducer and its driving circuits and increase a broadband energy transfer, it is expected that the pulse lengths can be shortened, increasing the axial resolution in a pulse-echo imaging (assuming that the dispersion is not significant, i.e., $\alpha \ll k_0$ in Eq. (6)) [64].

Finally, the method that uses a single high-voltage RF power amplifier in combination with an RF transformer to drive an annular array transducer to produce a Bessel beam can potentially be used for wearable medical ultrasound imaging [44]-[48] and wearable super-resolution imaging [49]-[52], as is shown in an example in Fig. 7(a), where the Bessel beam is used in both transmit and receive or is used in transmit and a dynamically focused beam is used in receive to reduce sidelobes and increase image contrast [38][65][67]. The transmit electronics in Fig. 7(a) is the same as that of Fig. 7(b) that is the simplest imaging system where a single-element focused transducer is used. However, the quality of images obtained with Fig. 7(a) will be much better than that obtained with Fig. 7(b) since the imaging system in Fig. 7(a) has a large depth of field. To form an image using an annular array transducer in Fig. 7(a), the ultrasound beam produced by the transducer needs to be steered mechanically [38][53][65]. Fig. 8 shows an example wearable treadmill stress echocardiographic imaging system [66][67] that uses an annular array transducer to produce a Bessel beam and a reflector [54][55] that can be vibrated in multiple directions with at least two orthogonal electromagnets, micro motors such as micro stepper motors with attached or embedded encoders, or a combination of electromagnets and micro motors to steer the beam to form 3D or multi-plane 2D images. For super-resolution imaging, a modulator can be produced with a focused Bessel beam to modulate the phase of subsequent imaging waves [49]-[52].

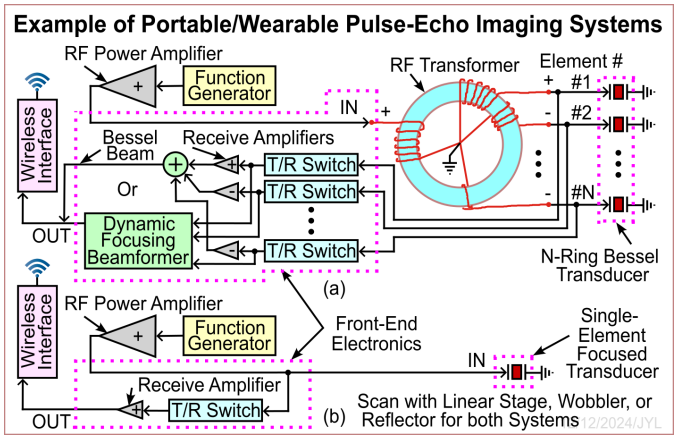

Fig. 7. An example of pulse-echo imaging systems using a pulse Bessel beam or a conventional focused beam. (a) An imaging system that uses a single high-voltage RF power amplifier in combination with an RF transformer to produce a pulse Bessel beam of a large depth of field. The received signals obtained via T/R switches are combined to produce a Bessel beam response or

a conventional dynamically focused beam (such as Gaussian beam) to reduce sidelobes. The combined or beamformed signal can then be transmitted wirelessly to a remote device such as a computer or a mobile phone for image display or be processed for image display on a local device. Images can be formed by scanning the beams with a wobbler [38][53] or a vibrating reflector [54][55]. (b) The simplest imaging system that uses the same single high-voltage RF power amplifier and a single-element transducer focused at a fixed distance in both transmit and receive for comparison with (a). Note that although both imaging systems could have a similar power consumption, size, and weight, the imaging system in (b) has a much shorter depth of field and thus poorer image quality.

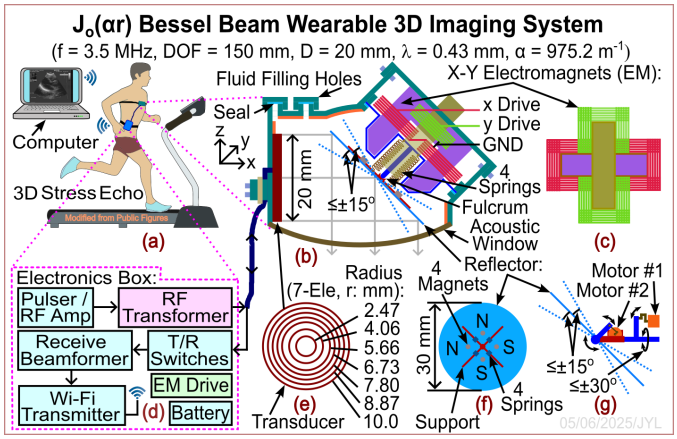

Fig. 8. An example of a battery-operated wearable 3D or multi-plane ultrasound imaging system using a Bessel beam that is produced with an RF transformer and a reflector that can vibrate in multiple directions. (a) An illustration of 3D or multi-plane heart imaging during a treadmill exercise. (b) A Bessel transducer module that is attached to the chest of the patient in (a). (c) Two orthogonal electromagnets used to vibrate the reflector to steer the Bessel beam. (d) A block diagram of electronics box that contains a pulser / RF amplifier, an RF transformer, T/R switches, a beamformer, a Wi-Fi transmitter, a driver for electromagnets or micro step motors (EM), and a battery. The electronics box can be strapped on the waist of the patient and the beamformed data can be transmitted through Wi-Fi and displayed on the computer in (a) or a mobile phone. (e) A 20-mm diameter, 7-element (ring), and 3.5-MHz annular array transducer. The transducer can be used to produce a Bessel beam of a depth of field of 150 mm in both transmit and receive, or can be used to produce a Bessel beam in transmit and a dynamically focused beam in receive to reduce sidelobes. (f) A thin ultrasound reflector that contains 4 small magnets and 4 small springs. The reflector is supported at the center via a fulcrum and can vibrate in multiple directions to form 2D images in multiple planes or a 3D image. (g) Vibrating the reflector using micro stepper motors with attached or embedded encoders instead of electromagnets for a precise motion control (the reflector can be moved in multiple directions as indicated by the curved arrows without the center fulcrum, magnets, and springs). Note that a combination of electromagnets and micro motors also can be used to vibrate the reflector. Other parameters of the imaging system are in the subtitle of the figure.

VI. Conclusion

A method that uses a single high-voltage RF power amplifier in combination with an RF transformer to drive an annular array transducer was developed to produce pulse Bessel beams that have a large depth of field [5]. This method simplifies the electronics used to drive the annular array transducer and reduces their power, size, and weight, making it easer to apply the Bessel beams to wearable medical ultrasound imaging [44]-[48] or wearable super-resolution imaging [49]-[52]. Experiments were performed with a 10-ring, 50-mm diameter, 2.5-MHz center frequency, and broadband (about 72% -6 dB relative one-way bandwidth) annual array transducer. The RF transformer was custom made and was consisted of one primary and 10 secondary windings. The results show that pulse Bessel beams of a small beamwidth of about 2.53 mm (4.22 wavelengths) and a large depth of field of about 216 mm (about 360 wavelengths) can be produced with the new method. In addition, examples were given to show how the new method can be applied to wearable 3D or multi-plane 2D ultrasound imaging [44]-[48] and super-resolution imaging [49]-[52] by steering the beam mechanically with a reflector [54][55] that can vibrate in multiple directions.

Acknowledgment

The author would like to thank Dr. Pengfei Song of Duke University and Dr. Sheng Xu of the University of California at San Diego for discussions on the potential of the method developed in this paper for wearable applications. The author would also like to thank Dr. Samer Khouri of The University of Toledo for a discussion on possible applications of the method in echocardiography.

References

[1] J. A. Stratton, *Electromagnetic Theory*. New York and London: McGraw-Hill Book Company, 1941, Page 356.

[2] Durnin, J. "Exact solutions for nondiffracting beams. I. The scalar theory." *JOSA A* 4, no. 4 (1987): 651-654.

[3] J. Durnin, J. J. Miceli Jr, and J. H. Eberly. "Diffraction-free beams." *Physical review letters* 58, no. 15 (1987): 1499.

[4] J. Durnin, J. J. Miceli Jr, and J. H. Eberly. "Experiments with nondiffracting needle beams." In *International Quantum Electronics Conference*, p. FHH5. Optica Publishing Group, 1987.

[5] Jian-yu Lu and J. F. Greenleaf, "Ultrasonic nondiffracting transducer for medical imaging," *IEEE Transactions on Ultrasonics, Ferroelectrics, and Frequency Control*, vol. 37, no. 5, pp. 438-447, September 1990.

[6] X. Chu. "Analytical study on the self-healing property of Bessel beam." *The European Physical Journal D* 66 (2012): 1-5.

[7] Jian-yu Lu and J. F. Greenleaf, "Pulse-echo imaging using a nondiffracting beam transducer," *Ultrasound in Medicine and Biology*, vol. 17, no. 3, pp. 265-281, May 1991.

[8] Jian-yu Lu, H. Zou, and J. F. Greenleaf, "Biomedical ultrasound beam forming," *Ultrasound in Medicine and Biology*, vol. 20, no. 5, pp. 403-428, July 1994.

[9] Jian-yu Lu, J. Cheng, and B. C. Cameron, "Low sidelobe limited diffraction optical coherence tomography," in *Coherence Domain Optical Methods in Biomedical Science and Clinical Applications VI*, Valery V. Tuchin, Joseph A. Izatt, James G. Fujimoto, Editors, *Proceedings of SPIE*, vol. 4619, pp. 300-311, 2002.

[10] N. Wang and J. Yao. "Sound Out the Deep Clarity: Super-resolution Photoacoustic Imaging at Depths." *IEEE Transactions on Ultrasonics, Ferroelectrics, and Frequency Control* (2024).

[11] Jian-yu Lu, X.-L. Xu, H. Zou, and J. F. Greenleaf, "Application of Bessel beam for Doppler velocity estimation," *IEEE Transactions on Ultrasonics, Ferroelectrics, and Frequency Control*, vol. 42, no. 4, pp. 649-662, July 1995.

[12] Jian-yu Lu and J. F. Greenleaf, "Diffraction-limited beams and their applications for ultrasonic imaging and tissue characterization," in *New Developments in Ultrasonic Transducers and Transducer Systems*, F. L. Lizzi, Editor, *Proceedings of SPIE*, vol. 1733, pp. 92-119, 1992.

[13] Jian-yu Lu and J. F. Greenleaf, "Producing deep depth of field and depth-independent resolution in NDE with limited diffraction beams," *Ultrasonic Imaging*, vol. 15, no. 2, pp. 134-149, April 1993.

[14] Jian-yu Lu, "Designing limited diffraction beams," *IEEE Transactions on Ultrasonics, Ferroelectrics, and Frequency Control*, vol. 44, no. 1, pp. 181-193, January 1997.

[15] Jian-yu Lu, "Focused limited-diffraction beams for ultrasound therapy applications," in *2021 IEEE International Ultrasonics Symposium Proceedings*, pp.1-4, 2021.

[16] F. G. Mitri. "Single Bessel tractor-beam tweezers." *Wave Motion* 51, no. 6 (2014): 986-993.

[17] T. A. Moura, U. M. S. Andrade, J. B. S. Mendes, and M. S. Rocha. "Modulating the trapping and manipulation of semiconductor particles using Bessel beam optical tweezers." *Optics and Lasers in Engineering* 170 (2023): 107778.

[18] S. Jiménez-Gambín, N. Jiménez, J. M. Benlloch, and F. Camarena. "Generating Bessel beams with broad depth-of-field by using phase-only acoustic holograms." *Scientific reports* 9, no. 1 (2019): 20104.

[19] S. Lin, Li Gong and Z. Huang. "Super‐Resolution Two‐Photon Fluorescence Tomography Through the Phase‐Shifted Optical Beatings of Bessel Beams for High‐Resolution Deeper Tissue 3D Imaging." *Laser & Photonics Reviews* 18, no. 2 (2024): 2300634.

[20] T. Meinert and A. Rohrbach. "Light-sheet microscopy with length-adaptive Bessel beams." *Biomedical optics express* 10, no. 2 (2019): 670-681.

[21] H. Kim, K. Mishchik, A. Voronov, J. Kim, W. Jung, J. You, S. Jang, S. Park, K. Yoo, S. Baek, J. Ryu, S. Jeong, C. Roh. "Optimization of Bessel beam optics for high-quality glass cutting." In *Laser-based Micro-and Nanoprocessing XVI*, vol. 11989, pp. 6-17. SPIE, 2022.

[22] Z. Lu, Z. Guo, M. Fan, M. Guo, C. Li, Y. Yao, H. Zhang, W. Lin, H. Liu, and B. Liu. "Tunable bessel beam shaping for robust atmospheric optical communication." *Journal of Lightwave Technology* 40, no. 15 (2022): 5097-5106.

[23] D. Y. Vasylyev, A. A. Semenov, and W. Vogel. "Toward global quantum communication: beam wandering preserves nonclassicality." *Physical review letters* 108, no. 22 (2012): 220501.

[24] M. McLaren, M. Agnew, J. Leach, F. S. Roux, M. J. Padgett, R. W. Boyd, and A. Forbes. "Entangled bessel-gaussian beams." *Optics express* 20, no. 21 (2012): 23589-23597.

[25] M. McLaren, T. Mhlanga, M. J. Padgett, F. S. Roux, and A. Forbes. "Self-healing of quantum entanglement after an obstruction." *Nature communications* 5, no. 1 (2014): 3248.

[26] L. Schächter and W. D. Kimura. "Electron beam guiding by a laser Bessel beam." *Physical Review Accelerators and Beams* 23, no. 8 (2020): 081301.

[27] B. Hafizi, E. Esarey, and P. Sprangle. "Laser-driven acceleration with Bessel beams." *Physical Review E* 55, no. 3 (1997): 3539.

[28] D. Mugnai and P. Spalla. "Electromagnetic propagation of Bessel-like localized waves in the presence of absorbing media." *Optics communications* 282, no. 24 (2009): 4668-4671.

[29] O. Brzobohatý, T. Čižmár, and P. Zemánek. "High quality quasi-Bessel beam generated by round-tip axicon." *Optics express* 16, no. 17 (2008): 12688-12700.

[30] M. A. Mahmoud, M. Y. Shalaby, and D. Khalil. "Propagation of Bessel beams generated using finite-width Durnin ring." *Applied optics* 52, no. 2 (2013): 256-263.

[31] N. Jiménez, R. Picó, V. Sánchez-Morcillo, V. Romero-García, L. M. García-Raffi, and K. Staliunas. "Formation of high-order acoustic Bessel beams by spiral diffraction gratings." *Physical Review E* 94, no. 5 (2016): 053004.

[32] Jian-yu Lu and J. F. Greenleaf, "Nondiffracting X waves --- exact solutions to free-space scalar wave equation and their finite aperture realizations," *IEEE Transactions on Ultrasonics, Ferroelectrics, and Frequency Control*, vol. 39, no. 1, pp. 19-31, January 1992.

[33] N. Chattrapiban, E. A. Rogers, D. Cofield, W. T. Hill III, and R. Roy. "Generation of nondiffracting Bessel beams by use of a spatial light modulator." *Optics letters* 28, no. 22 (2003): 2183-2185.

[34] Q. Zhang, X. M. Cheng, H. W. Chen, B. He, Z. Y. Ren, Y. Zhang, and J. T. Bai. "Diffraction-free, self-reconstructing Bessel beam generation using thermal nonlinear optical effect." *Applied Physics Letters* 111, no. 16 (2017).

[35] P. Steinvurzel, K. Tantiwanichapan, M. Goto, and S. Ramachandran. "Fiber-based Bessel beams with controllable diffraction-resistant distance." *Optics letters* 36, no. 23 (2011): 4671-4673.

[36] J. A. Campbell and S. Soloway. "Generation of a nondiffracting beam with frequency‐independent beamwidth." *The Journal of the Acoustical Society of America* 88, no. 5 (1990): 2467-2477.

[37] D. K. Hsu, F. J. Margetan, and D. O. Thompson. "Bessel beam ultrasonic transducer: Fabrication method and experimental results." *Applied physics letters* 55, no. 20 (1989): 2066-2068.

[38] Jian-yu Lu, T.-K. Song, R. R. Kinnick, and J. F. Greenleaf. "In vitro and in vivo real-time imaging with ultrasonic limited diffraction beams." *IEEE transactions on medical imaging* 12, no. 4 (1993): 819-829.

[39] J. Saito and H. Nomura. "Realization of an ultrasonic Bessel-like beam using a single-system-driven multi-annular source with controlled vibrational area." *Japanese Journal of Applied Physics* 64, no. 3 (2025): 03SP08.

[40] C. B. Burckhardt, H. Hoffmann, and P-A. Grandchamp. "Ultrasound axicon: a device for focusing over a large depth." *The Journal of the Acoustical Society of America* 54, no. 6 (1973): 1628-1630.

[41] M. Moshfeghi. "Sidelobe suppression in annular array and axicon imaging systems." *The Journal of the Acoustical Society of America* 83, no. 6 (1988): 2202-2209.

[42] Y. Zhao, H. Y. Dong, S. Zhao, S. Min, J. Cheng, B. Li, F. Chi, and S. Liu. "Design of broadband impedance-matching Bessel lens with acoustic metamaterials." *Journal of Applied Physics* 126, no. 6 (2019).

[43] Jian-yu Lu and J. F. Greenleaf, "A study of two-dimensional array transducers for limited diffraction beams," *IEEE Transactions on Ultrasonics, Ferroelectrics, and Frequency Control*, vol. 41, no. 5, pp. 724-739, September 1994.

[44] H. Huang, R. S. Wu, M. Lin, and S. Xu. "Emerging wearable ultrasound technology." *IEEE Transactions on Ultrasonics, Ferroelectrics, and Frequency Control* 71, no. 7 (2023): 713-729.

[45] H. Hu, H. Huang, M. Li, X. Gao, L. Yin, R. Qi, R. S. Wu, X. Chen, Y. Ma1, K. Shi, C. Li, T. M. Maus, B. Huang, C. Lu, M. Lin, S. Zhou, Z. Lou, Y. Gu, Y. Chen, Y. Lei, X. Wang, R. Wang, W. Yue, X. Yang, Y. Bian, J. Mu, G. Park, S. Xiang, S. Cai, P. W. Corey, J. Wang, and S. Xu. "A wearable cardiac ultrasound imager." *Nature* 613, no. 7945 (2023): 667-675.

[46] X. Gao, X. Chen, M. Lin, W. Yue, H. Hu, S. Qin, F. Zhang, Z. Lou, L. Yin, H. Huang, S. Zhou, Y. Bian, X. Yang, Y. Zhu, J. Mu, X. Wang, G. Park, C. Lu, R. Wang, R. S. Wu, J. Wang, J. Li, and S. Xu. "A wearable echomyography system based on a single transducer." *Nature Electronics* (2024): 1-12.

[47] M. Lin, Z. Zhang, X. Gao, Y. Bian, R. S. Wu, G. Park, Z. Lou, Z. Zhang, X. Xu, X. Chen, A. Kang, X. Yang, W. Yue, L. Yin, C. Wang, B. Qi, S. Zhou, H. Hu, H. Huang, M. Li, Y. Gu, J. Mu, A. Yang, A. Yaghi, Y. Chen, Y. Lei, C. Lu, R. Wang, J. Wang, S. Xiang, E. B. Kistler, N. Vasconcelos, and S. Xu. "A fully integrated wearable ultrasound system to monitor deep tissues in moving subjects." *Nature biotechnology* 42, no. 3 (2024): 448-457.

[48] S. Zhou, X. Gao, G. Park, X. Yang, B. Qi, M. Lin, H. Huang, Y. Bian, H. Hu, X. Chen, R. S. Wu, B. Liu, W. Yue, C. Lu, R. Wang, P. Bheemreddy, S. Qin, A. Lam, K. A. Wear, M. Andre, E. B. Kistler, D. W. Newell, and S. Xu. "Transcranial volumetric imaging using a conformal ultrasound patch." *Nature* 629, no. 8013 (2024): 810-818.

[49] Jian-yu Lu, "Modulation of Point Spread Function for Super-Resolution Imaging." *IEEE Transactions on Ultrasonics, Ferroelectrics, and Frequency Control* , vol. 71, no. 1, pp. 153-177, January 2024.

[50] Jian-yu Lu, "A general method to obtain clearer images at a higher resolution than theoretical limit," 186th Meeting of Acoustical Society of America, Acoustical Lay Language Paper, April 22, 2024 (https://acoustics.org/a-general-method-to-obtain-clearer-images-at-a-higher-resolution-than-theoretical-limit/).

[51] Jian-yu Lu, "Remote Super-Resolution Mapping of Wave Fields," *IEEE Transactions on Ultrasonics, Ferroelectrics, and Frequency Control*, vol. 72, no. 3, pp. 370-379, March 2025.

[52] Jian-yu Lu, "Generation of modulators for super-resolution imaging," *Journal of Acoustical Society of America*, vol. 157 no. 4, pt. 2, pp. A56, 2025 (abs) (https://doi.org/10.1121/10.0037370).

[53] B. S. Verma. "Ultrasound Transducers and Image Quality." *IETE Technical Review* 9, no. 2 (1992): 128-133.

[54] Z. Dong, S. Li, M. R. Lowerison, J. Pan, J. Zou, and P. Song. "Fast acoustic steering via tilting electromechanical reflectors (FASTER): A novel method for high volume rate 3-D ultrasound imaging." *IEEE transactions on ultrasonics, ferroelectrics, and frequency control* 68, no. 3 (2021): 675-687.

[55] Z. Dong, S. Li, X. Duan, M. R. Lowerison, C. Huang, Q. You, S. Chen, J. Zou, and P. Song. "High-Volume-Rate 3-D Ultrasound Imaging Using Fast-Tilting and Redirecting Reflectors." *IEEE transactions on ultrasonics, ferroelectrics, and frequency control* 70, no. 8 (2023): 799-809.

[56] X. Chen, F. Dong, C. Yin, J. Tu, D. Zhang, and X. Guo. "Ultrasonic imaging based on pulsed Airy beams." *IEEE Transactions on Ultrasonics, Ferroelectrics, and Frequency Control* 70, no. 9 (2023): 1146-1156.

[57] F. S. Foster, M. S. Patterson, M. Arditi, and J. W. Hunt. "The conical scanner: a two transducer ultrasound scatter imaging technique." *Ultrasonic imaging* 3, no. 1 (1981): 62-82.

[58] S. C. Gupta, "Delta function." *IEEE Transactions on Education* 1 (1964): 16-22.

[59] Jian-yu Lu . Multi-Channel Data Transmission with X Wave and Bessel Pulses. *TechRxiv.* March 02, 2023. (DOI: https://doi.org/10.36227/techrxiv.22083719.v2).

[60] Jian-yu Lu. "Limited-Diffraction Beams for Secure Fast Data Communications." In *2023 IEEE International Ultrasonics Symposium (IUS)*, pp. 1-4. IEEE, 2023.

[61] D. J. Griffiths. *Introduction to electrodynamics*. Cambridge University Press, 2023.

[62] Jian-yu Lu and J. Cheng, "Field computation for two-dimensional array transducers with limited diffraction array beams," *Ultrasonic Imaging*, vol. 27, no. 4, pp. 237-255, October 2005.

[63] Jian-yu Lu and J. F. Greenleaf, "Experimental verification of nondiffracting X waves," *IEEE Transactions on Ultrasonics, Ferroelectrics, and Frequency Control*, vol. 39, no. 3, pp. 441-446, May 1992.

[64] H. Zhou, S. H. Huang, and Wei Li. "Electrical impedance matching between piezoelectric transducer and power amplifier." *IEEE Sensors Journal* 20, no. 23 (2020): 14273-14281.

[65] W. Qiu, Y. Yu, H. R. Chabok, C. Liu, F. K. Tsang, Q. Zhou, K. K. Shung, H. Zheng, and L. Sun. "A flexible annular-array imaging platform for micro-ultrasound." *IEEE transactions on ultrasonics, ferroelectrics, and frequency control* 60, no. 1 (2013): 178-186.

[66] B. T. Fitzgerald, J. J. Presneill, I. G. Scalia, C. L. Hawkins, Y. Celermajer, W. M. Scalia, and G. M. Scalia. "The prognostic value of the diastolic stress test in patients undergoing treadmill stress echocardiography." *Journal of the American Society of Echocardiography* 32, no. 10 (2019): 1298-1306.

[67] Jian-yu Lu and Samer Khouri, "Imaging systems, beam generators, and beam steering modules," *United States Patent (provisional) pending*, No. 63/846,311.

Jian-yu Lu (S'86--M'88--SM'99--F'08--LF'25) received the B.S. degree in physics/electrical engineering from Fudan University, Shanghai, China, in February 1982; the M.S. degree in physics/acoustics from Tongji University, Shanghai, China, in 1985; and the Ph.D. degree in biomedical engineering from Southeast University, Nanjing, China, in 1988.

From December 1988 to February 1990, he was a Postdoctoral Research Fellow with the Mayo Medical School, Rochester, Minnesota, USA. Later, he was an Associate Professor of biophysics with the Mayo Medical School and an Associate Consultant with the Department of Physiology and Biophysics, Mayo Clinic/Foundation, Rochester, Minnesota, USA. Since 1997, he has been a full Professor with the Department of Bioengineering, The University of Toledo (UT), Toledo, OH, USA, where he also has been an Adjunct Professor with the College of Medicine and Life Sciences, since 1998. His research interests are in acoustic imaging, devices, tissue identification; medical ultrasonic transducers; ultrasonic beam forming; and wave propagation physics.

Dr. Lu is a Fellow of IEEE (conferred in 2008), a Fellow of the American Institute of Ultrasound in Medicine (AIUM) (conferred in 2005), and a Fellow of the American Institute for Medical and Biological Engineering (AIMBE) (conferred in 2007). He received the Outstanding Paper Award from the IEEE UFFC Society (UFFC-S) for two of his papers published in the IEEE Transactions on Ultrasonics, Ferroelectrics, and Frequency Control (TUFFC) in 1992 for the discovery of X wave that, in theory, is both diffraction and dispersion free. Both phase and group velocities of the X wave are faster than the speed of sound (supersonic) or light in vacuum (superluminal) (see newly-developed superluminal X wave in quantum mechanics in 2023 at IEEE TechRxiv https://doi.org/10.36227/techrxiv.22083719.v2 and 2023 IEEE IUS https://doi.org/10.1109/IUS51837.2023.10306675). In addition, he received the Edward C. Kendall Award for his meritorious research from the Mayo Alumni Association in 1992, the NIH FIRST Award in 1991, the Distinguished Service Award from UFFC-S in 2016, and the Engineer of the Year Award from the IEEE Toledo Section in 2021. Also, in medical ultrasound, he first developed the plane-wave 2D and 3D high-frame-rate imaging in 1997 (https://doi.org/10.1109/58.655200) and first produced an ultrasound Bessel beam with an annular array transducer in 1990 (https://doi.org/10.1109/58.105250).

Dr. Lu served as the President of IEEE UFFC-S from 2014 to 2015, the Editor-in-Chief of IEEE TUFFC from 2002 to 2007, the General Chair of the 2008 IEEE International Ultrasonics Symposium (IUS), the Technical Program Committee (TPC) Chair of 2001 IEEE IUS, a member of the Editorial Board of IEEE Access from 2016 to 2021, an Elected AdCom member of IEEE UFFC-S from 2009 to 2011, and many committees of UFFC-S. In addition, he served in IEEE Toledo Section.